Femtosecond photon echo measurements of electronic coherence relaxation between the $X(^1\Sigma_{g+})$ and $B(^3\Pi_{0u+})$ states of I_2 in the presence of He, Ar, N_2, O_2, C_3H_8

Matthew Comstock, Vadim V. Lozovoy, and Marcos Dantus[a)]
Department of Chemistry and Department of Physics and Astronomy, Michigan State University, East Lansing, Michigan 48824

(Received 29 July 2002; accepted 3 July 2003)

Photon echo and reverse transient grating measurements of the loss of electronic coherence for molecular iodine are presented. Systematic measurements of the coherence decay rate were made as a function of buffer gas. From the dependence of decay rate on numerical density, we calculated experimental cross sections of decoherence. These values range from 135 $Å^2$ for helium to 1170 $Å^2$ for I_2. We find Lennard-Jones parameters for the long-range interactions responsible for decoherence which can be modeled by dispersion forces. © *2003 American Institute of Physics.* [DOI: 10.1063/1.1603739]

I. INTRODUCTION

There is considerable theoretical and experimental interest in controlling the amplitude and phase of quantum mechanical states in atoms and molecules.[1–3] The motivation behind these efforts comes from evidence that intramolecular dynamics and chemical reactivity can be controlled using phase and amplitude shaped pulses.[4,5] A second motivation is the future construction of a computer that will operate through the coherent manipulation of individual quantum states.[6–8] For both of these applications, coherent interactions between the laser field and the atom or molecule are required. Here we explore the loss of electronic coherence in gas phase iodine molecules, a model system that has been explored for the coherent manipulation of information,[9,10] as a function of number density and the addition of different buffer gases. The rate of decoherence determines how long information can be manipulated without loss of fidelity. The loss of coherence and the nature of the long-range interactions between ultracold atoms and Bose–Einstein condensates has become a subject of recent interest.[11,12] Our measurements may help to shed light on that subject as well.

This work is a continuation of work from our laboratory, where we have used femtosecond three-pulse four-wave mixing (FWM) methods, involving different pulse sequences, to measure many of the processes that contribute to coherence relaxation in ground and excited state iodine.[13–16] We make the distinction between different measurements, such as electronic coherence decay (involving two electronic states), from vibrational or rotational coherence decay (involving vibrations or rotational motion in a given electronic state), and spatial coherence decay (involving the motion of atoms or molecules in space). The focus of this report is on the nature of interactions (long-range collisions) that lead to a loss of electronic coherence (decoherence). For our measurements, we ignore the lifetime of the upper electronic state, T_1, because it is in the microsecond time scale. Our measurements involve pure iodine as well as iodine in the presence of buffer gases that range from He atoms to propane molecules.

The signal measured from coherent spectroscopic methods, such as FWM, depends on phase coherence among all molecules emitting the field. As the phase coherence is lost the strength of the signal diminishes. Measuring the rate of decoherence and understanding the nature of the interactions that cause it in gas phase environments are the goals of this work. In the gas phase, decoherence typically results from long-range interactions, which cause a phase change in the polarization of the single molecule. In Fig. 1, we consider an iodine molecule in an electronic coherence between the $B(^3\Pi_{0u}^+)$ and the $X(^1\Sigma_g^+)$ states, the potential energy curves for the relevant electronic states are shown. The molecule, whose polarization oscillates with frequency ω, can be perturbed through long range interactions with buffer gas molecules. This perturbation changes the energy of the B and X states and result in a time dependent frequency change $\Delta\omega(t)$. The accumulated phase change $\Delta\varphi$ that results from one such long-range interaction leads to the measured dephasing as the emitted electric field destructively interferes with the emitted fields from other molecules in the sample.

In this study, we use two types of pulse sequences: photon echo (PE) and reverse transient grating (RTG).[17] Both methods measure the electronic coherence decay that results from the first order polarization $\rho^{(1)}$ (see Fig. 2); however, they have a very different dependence on homogeneous and inhomogeneous contributions. In condensed phases, the inhomogeneous contribution to coherence loss is very significant making PE measurements the only viable method to obtain measurements of electronic coherence decay in the condensed phase. In the gas phase, inhomogeneous contributions are much smaller; therefore, both PE and RTG can provide valuable information. In principle, for very low pressures and small molecules it is possible to measure the Doppler free linewidth of individual spectroscopic transitions to

a)Author to whom correspondence should be addressed. Electronic mail: dantus@msu.edu

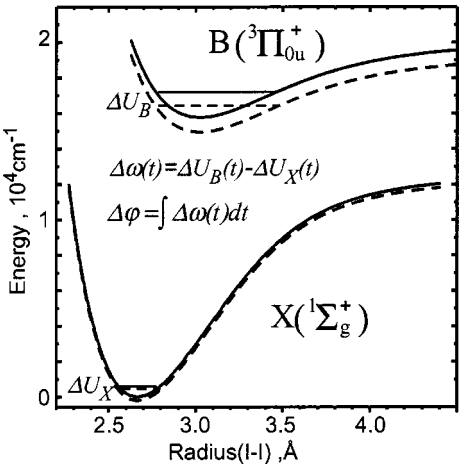

FIG. 1. A graph of the potential energy curves (solid line) involved in the electronic coherence between the B and X states of iodine. Dashed lines represent the perturbation caused by the approaching buffer gas molecule. The overall change in energy is indicated by $\Delta\omega$. The phase shift $\Delta\varphi$ necessary to destroy the coherence during a long-range collision is given by the accumulated phase shift taking place during the interaction.

estimate the pure homogeneous broadening. However, for room temperature iodine in the presence of buffer gases, time-resolved measurements as performed here are clearly advantageous and provide both homogeneous and inhomogeneous decoherence rates. In the Theory, we describe the signals from the two methods and recover the isolated molecule and condensed phase limits. We later show in the Results that, under certain conditions, our measurements involve an intermediate case, between the two limits, that has not received much attention in the literature.

The article is organized as follows: Section II describes the theory behind PE and RTG measurements. Particular emphasis is placed on contrasting the response from liquid and gas phase samples. Section III describes the experimental setup used to carry out the measurements. Section IV presents the results and describes the data analysis. Section V presents a discussion of the observed results and places them in the context of measurements in other laboratories and estimates obtained from dispersion forces alone. Section VI summarizes our findings and general conclusions.

II. THEORY

The intensity of the PE signal as a function of delay time in the liquid phase has long been known to conform to an exponential decay with time constant $\frac{1}{4}T_2'$, where T_2' is the homogeneous relaxation time.[18] Similarly, it has been shown that for gas phase samples, the photon echo decays with rate $\frac{1}{2}T_2'$.[19] In this section, we explore the reason for the factor of 2 difference for these two limits, and develop a means of extracting T_2' even from the intermediate region where neither the gas phase nor the liquid phase limits apply.

To correctly describe the evolution of the system including relaxation and obtain an expression that bridges the gap between the liquid phase and the gas phase limits we use a density matrix approach. The formalism we use to describe PE and RTG is based on this approach published earlier.[20] Here we apply it to derive simple formulas for the intermediate between liquid and gas phase cases. For PE and RTG, the first pulse arrives at time zero while the second and third coincide in time, following after a delay τ. In the case of PE the emission goes in the phase matching direction $\mathbf{k}_{\mathrm{PE}}=\mathbf{k}_3+\mathbf{k}_2-\mathbf{k}_1$ (responses R_{II} and R_{III}), while in the case of RTG the emission goes in the phase matching direction $\mathbf{k}_{\mathrm{RTG}}=\mathbf{k}_3-\mathbf{k}_2+\mathbf{k}_1$ (responses R_{I} and R_{IV}),[21] as depicted in Fig. 2. There are no differences in amplitude between the Liouville pathways R_{I} and R_{IV} and between R_{II} and R_{III} for a two level system. Notice that the PE signal has a maximum at time 2τ. For RTG the maximum is at zero time (before the second pair of pulses, in the ''virtual'' unphysical region), as shown in Fig. 2. The difference between PE and RTG is very important when molecules within the ensemble have different resonance conditions because of inhomogeneities.

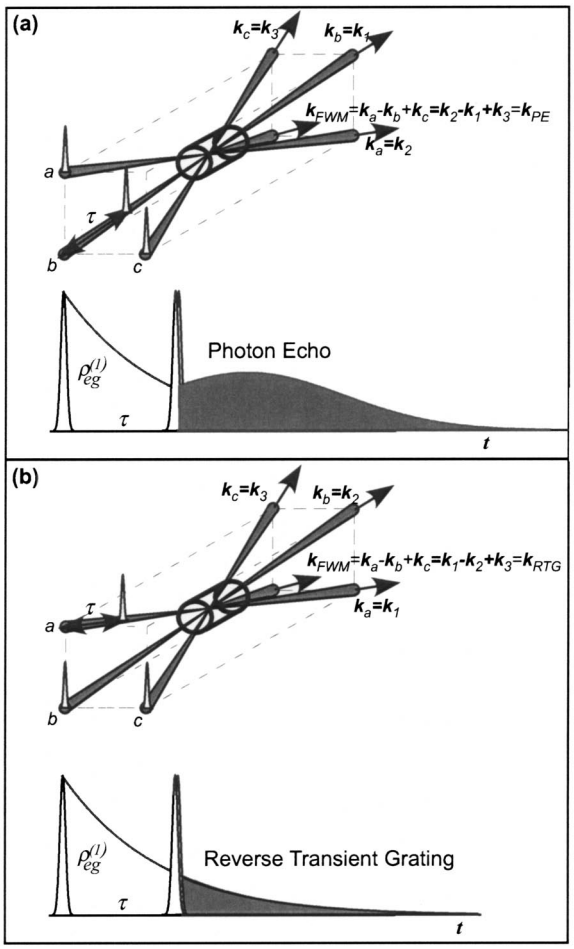

FIG. 2. Pulse sequence and phase-matching geometry for PE and RTG measurements. The PE setup (a) with pulse **b** arriving before pulses **a** and **c** undergoes rephasing and has a maximum at time τ after the second two pulses. The RTG (b) with pulse **a** arriving before pulses **b** and **c**, undergoes no rephasing and is thus maximum at the time of the second two pulses.

The inhomogeneous relaxation can be described by the normalized Gaussian spectral distribution $\exp[-(\omega-\omega_0)^2/\Delta^2]$ of each transition frequency with width Δ. The signal measured as a function of the delay τ corresponds to the temporal integral of the emission intensity. We can separate the electric field of the PE and RTG signals because they are generated in different directions. It is possible to analytically

calculate the relaxation in the case of an exponential homogeneous decay and a Gaussian inhomogeneous decay. For these cases we obtain

$$S_{\mathrm{PE}}(\tau) \propto \int_{\tau}^{\infty} \exp(-2\gamma t)\exp(-(t-2\tau)^2\Delta^2/2)dt$$
$$= \exp(2\gamma^2\Delta^{-2})[1-\mathrm{erf}(2^{-0.5}\tau\Delta + 2^{0.5}\gamma\Delta^{-1})]$$
$$\times (2/\pi)^{0.5}/\Delta, \quad (1)$$

$$S_{\mathrm{RTG}}(\tau) \propto \int_{\tau}^{\infty} \exp(-2\gamma t)\exp(-t^2\Delta^2/2)dt$$
$$= \exp(2\gamma^2\Delta^{-2} - 4\tau\gamma)[1+\mathrm{erf}(2^{-0.5}\tau\Delta$$
$$- 2^{0.5}\gamma\Delta^{-1})](2/\pi)^{0.5}/\Delta. \quad (2)$$

The first exponent for both cases is the homogeneous decay (2γ is decay rate is twice of density elements decay). The second Gaussian function ($\Delta^2/2$ is twice faster of Fourier image of inhomogeneous distribution of frequency domain) is centered at time 2τ for the PE (echo spike) and at zero time for the RTG (inhomogeneous dephasing).

We define the homogeneous relaxation time in terms of the relaxation rate $T_2' = 1/\gamma$ and the inhomogeneous relaxation time in terms of the inhomogeneous spectral width $T_2^* = 1/\Delta$. In the limit $\tau T_2' \ll T_2^{*2}$ there is no difference between the PE and RTG signals. In this case, Eqs. (1) and (2) can be simplified to obtain

$$S_{\mathrm{PE}}(\tau) = S_{\mathrm{RTG}}(\tau) \propto \exp(-2\tau\gamma) = \exp(-2\tau/T_2'). \quad (3)$$

In the opposite case $\tau T_2' \gg T_2^{*2}$, the liquid phase limit, there is a difference between the PE and RTG signals. We can replace the integral formula for the PE Gaussian field with a delta function at time 2τ and get a simple decay with rate 4γ. In this case Eqs. (1) and (2) can be written as follows:

$$S_{\mathrm{PE}}(\tau) \propto \exp(-4\tau\gamma) = \exp(-4\tau/T_2'), \quad (4)$$

$$S_{\mathrm{RTG}}(\tau) \propto \exp(-\tfrac{1}{2}\Delta^2\tau^2) = \exp(-\tau^2/2T_2^{*2}). \quad (5)$$

Note that for short time delays, τ, the product $\tau T_2'$ is always small. Therefore, for small delays we expect the gas phase limit to be a good approximation. For large τ, the gas phase limit is no longer accurate even for gas phase experiments. Figure 3 demonstrates this transition between two limits. Note that initially the PE has a decay rate of 2γ, then goes through an intermediate region and, finally, at long delay times, has a rate of 4γ. In the case of RTG, the initial exponential decay with rate 2γ transforms to a faster Gaussian decay. For neat iodine at small density we found the PE and RTG signal decays are dramatically different; exponential for PE and Gaussian for RTG.[16] In the case of high density buffer gas or very short time, homogeneous dephasing is faster than inhomogeneous dephasing, making PE and RTG decay with approximately equal rates (2γ). This condition was accomplished for experiments with relatively high pressure of buffer gas and is different from the previous work from our group, where the homogeneous dephasing much slower.[16]

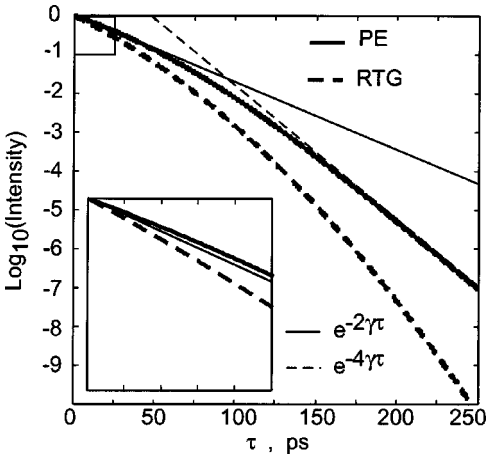

FIG. 3. Calculated PE and RTG decays ($\gamma = 2\times10^{10}\,\mathrm{s}^{-1}$ and $\Delta = 2\times10^{10}\,\mathrm{s}^{-1}$) showing both gas and liquid phase limits. At short times, both PE and RTG approach the gas phase limit (thin-solid line), at longer times, PE follows the liquid phase limit (thin-dashed line), and RTG decays nonexponentially.

III. EXPERIMENT

The experiments were carried out using a colliding pulse mode-locked dye laser (CPM) pumped by a continuous wave intracavity doubled Nd:YVO_4 laser. The output of the CPM was centered at 620 nm and was amplified by a four stage dye amplifier pumped at 30 Hz with the second harmonic of a nanosecond Nd:YAG laser. For most measurements, a double pass prism pair compressor was used to obtain 60 fs pulses with an average energy of 0.3 mJ per pulse. For some experiments, requiring longer pulses, the bandwidth of the CPM was purposely narrowed to ~1 nm and shifted to 615 nm. The fourth stage of the amplifier was double-passed, producing pulses that were 1.2 ps in duration with average pulse energy of 1 mJ. Pulse durations were determined by autocorrelation in a second harmonic generation crystal.

The laser was split into three beams of equal intensity, which were attenuated to less than 80 μJ per pulse (short pulse mode) or less than 300 μJ per pulse (long pulse mode) and recombined at the sample in the forward box geometry[22,23] (see Fig. 2). The beams occupy three corners of a 25 mm square and were determined to be parallel over one meter by using a template of the appropriate geometry. A 50 mm diameter, 0.5 m focal length lens focused the beams into the sample cell, the beams crossing at an angle of 2.9°. This crossing angle produces a transient grating with a 16 μm spacing. At the temperatures used in our measurements, the transient decays by diffusion after 60 ns. This time scale is three orders of magnitude longer than the coherence decay times being determined and is therefore neglected.

A computer-controlled actuator delayed the first beam, and the other two beams were overlapped in time. The pulse sequence defines the physical emission process which we detect in phase matching direction $\mathbf{k}_{\mathrm{FWM}} = \mathbf{k}_a - \mathbf{k}_b + \mathbf{k}_c$ (see Fig. 2). By changing the arrangement of the beams at the lens we controlled whether beam **b** or beam **a** was first. PE measurements with $\mathbf{k}_{\mathrm{PE}} = -\mathbf{k}_1 + \mathbf{k}_2 + \mathbf{k}_3$ require beam **b** to arrive at the sample before beams **a** and **c**, while RTG measurements with $\mathbf{k}_{\mathrm{RTG}} = \mathbf{k}_1 - \mathbf{k}_2 + \mathbf{k}_3$ require beam **a** to arrive

before beams **b** and **c**.[13] Time zero for both beam arrangements occurs when all three beams are overlapped in time. The temporal overlap of the beams was found using a removable 0.1 mm thick quartz plate.

The signal beam was collimated with a 0.5 m focal length lens, identical to the one that initially focuses the beams, and was spatially filtered through a 50 μm pinhole before being sent to a 0.27 m monochromator for detection (homodyne) by a photomultiplier tube. Data for the short pulse laser was collected at 620 nm, and for the long pulse laser data was collected at 615 nm. Both detection wavelengths represent the center of the laser's Gaussian spectral profile in the particular laser arrangement to which they correspond. Data were collected using a boxcar integrator, averaging 30 laser pulses. The laser pulse intensity was monitored with a photodiode and pulses with energy outside 1.5 standard deviations from the mean energy were discarded. Typical data sets were averaged for at least ten scans of 300 time delays each.

Sample cells consisted of quartz cylinders 4 in. in length, with optical windows. The cells were pumped to 10^{-5} Torr while the solid iodine sample (Kodak Chemical) was frozen with dry ice. The sample cells were then thawed, refrozen and pumped out again. Buffer gases (AGA) were added at room temperature and buffer gas pressure was measured with a baratron on a sealed gas line. Optical density measurements were made using a CW intracavity doubled Nd:YVO_4 laser (532 nm) and a photodiode covered by a 530 ± 10 nm bandpass filter to exclude stray light. The number density of iodine in the neat iodine cell was determined by transmission using established iodine absorption cross-section data.[24] The Nd:YVO_4 laser was determined to be of sufficient bandwidth to blur any fine structure on the absorption curve. This was confirmed using an absorption spectrometer with resolution set to half the laser bandwidth. A curve of iodine numerical density versus temperature was created. Our measurement of the extinction coeficient, $\epsilon=813\pm20$ L mol^{-1} cm^{-1} is in excellent agreement with that of previous measurements: $\epsilon=810\pm24$ L mol^{-1} cm^{-1}.[24] Using O.D.$=\epsilon nl$ we calculated the number density, n. These data agreed favorably with measurements from two other sources[25,26] in the temperature region considered here. Buffer gas sample cells were all heated with a heating tape until the desired iodine number density was reached. For pure iodine measurements, the number density was varied from 1×10^{23} to 8×10^{23} m^{-3} by controlling the temperature of the sample cell. All measurements involving buffer gases were made at a number density of iodine 5×10^{23} m^{-3} and 110–120 °C.

IV. RESULTS

A. Experiments on neat iodine vapor

Photon echo traces obtained from pure iodine vapor were taken as a function of number density, using 60 fs laser pulses. Figure 4 shows a plot of the homogeneous relaxation rate, γ, as a function of number density. Each data point on this plot represents a PE data set at a specific temperature in the pure iodine cell. A typical data set involved the measurement of PE signal intensity as a function of time delay between the first pulse and the other two pulses. The inset is a typical PE data set plotted on a logarithmic scale. The PE decays were measured from $\tau=-10$ ps to as much as $\tau=800$ ps, with at least 300 data points per scan. The final data sets were the result of from 10 to as many as 100 averages, requiring approximately 4 h of acquisition time.

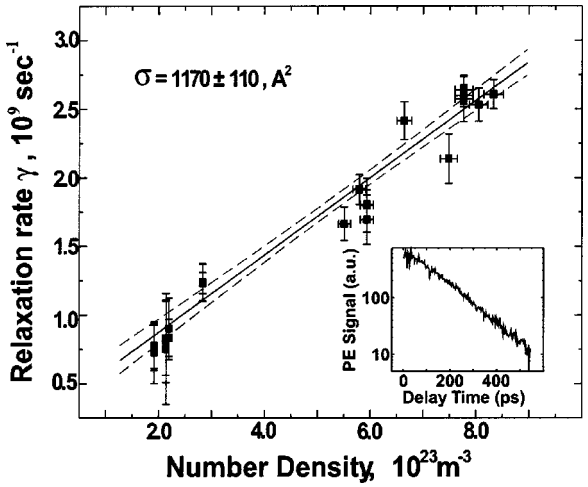

FIG. 4. Plot of homogeneous relaxation rate, γ, vs number density for neat iodine vapor. Results for 37 measurements are shown. Horizontal error bars indicate uncertainty in the absorption cross section of iodine, vertical error bars indicate uncertainty in the exponential fitting routine. Dotted lines represent the 90% confidence interval based on a linear least squares fit. Inset is a typical PE data trace plotted on a logarithmic scale. This trace corresponds to a number density of 5×10^{23} m^{-3}.

Experimental decays were fit to exponential decays of the form $\exp(-2\gamma\tau)$ to obtain γ. It has been verified previously that PE signals from gaseous iodine decay exponentially.[16,27] We use Eq. (3) to fit the PE data because the Doppler dephasing time T_2^* for iodine under these conditions is 720 ps, making the condition $\tau T_2' \ll T_2^{*2}$ valid. This was verified experimentally, as the RTG signal decays exponentially with a strong temperature dependence. The solid black line in Fig. 4 is a linear fit to the data, and the dotted lines represent the 90% confidence interval for that fit. Error bars in each dimension represent two standard deviations of the uncertainty of our measurements. Uncertainty in the decay rate comes directly from noise in the data set. Uncertainty in the number density is due to uncertainty in the absorption cross section of iodine. The uncertainty in the number density used in Fig. 4 results from the uncertainty in the absorption cross section reported previously.[24]

From a plot of coherence decay rate versus numerical density, we extract a cross section, σ, for electronic phase relaxation using the equation,

$$\gamma=n\sigma\bar{v}+\gamma_0, \tag{6}$$

where n is the number density of the gas sample, $\bar{v}$ is the average relative speed of the colliding molecules $\bar{v}=(8kT)^{1/2}(\pi\mu)^{-1/2}$, and γ_0 is the relaxation rate at zero pressure.

A fit through the experimental data in Fig. 4 allows us to determine a cross section of 1170 ± 110 Å^2 for neat iodine vapor, and a $1/\gamma_0$ of 58 ± 4 ns. This $1/\gamma_0$ value is in good

agreement with our estimation of the diffusional dephasing, 60 ns. The cross section obtained from Fig. 4 is in good agreement with the measurement obtained earlier in our group, 1150 ± 150 Å^2.[16] The electronic coherence decay cross section for iodine obtained by Zewail *et al.* is 590 ± 110 Å^2. This value differs from our findings by a factor of 2.[28] It is unclear how the T_2 values were obtained from the data in this reference. The difference could be explained if they obtained T_2' directly from the observed echo decay time without the factor of 2.

B. Experiments with buffer gases

Electronic coherence relaxation rates were measured as a function of number density for various buffer gases. The number density of iodine in the cell was monitored with a CW laser beam as described in the experimental section. PE transients were obtained for several buffer gas pressures for each of the different buffer gases. Each of the data sets was fit to Eq. (3) [single exponential decay with lifetime $1/(2\gamma)$, and γ values were extracted]. These data are shown in Fig. 5 for PE in the presence of He, Ar, O_2, and N_2. The solid lines are linear fits to the data, from which coherence relaxation cross sections were extracted [see formula (6)] and collected in Table I. Error bars represent the 90% confidence limits for each data point based on the uncertainty in the fit. Error in the pressure of the buffer gas is smaller than the data points, about ±2 Torr. For all cases the data points fall within the linear fit taking into account the uncertainty in the measurement. Values for γ were also extracted using Eqs. (1) and (2) (to take into account inhomogeneous broadening), with a two-dimensional nonlinear least squares fitting method. These γ values agree with the values extracted using Eq. (3) to within experimental error.

C. Photon echo and reverse transient grating measurements

For all the gaseous samples we measured both PE and RTG transients. RTG measurements are helpful in determining the inhomogeneous contribution to the relaxation rate, Δ (see Theory). In Fig. 6 we present data obtained with 5×10^{23} iodine molecules per cubic meter and 2.5×10^{24} propane molecules per cubic meter. Data were taken using 1.2 ps pulses to blur the vibrational dynamics of the coherence. This allowed us to obtain a smooth decay across the entire temporal range. The dots are experimental signal intensities plotted as a function of delay time τ. The solid lines are fits using Eqs. (1) and (2), and the dashed lines are exponential decays (pure homogeneous dephasing) using the γ determined by the same fit. The difference between PE and RTG decay times is small and within the experimental error. Similarly, the fits obtained from the theory [Eqs. (1) and (2) for the PE and RTG] and the simulations obtained from the single exponential decay [Eq. (3)] are within experimental error.

Figure 7 shows data points obtained from 37 independent transients for PE and RTG in the presence of propane at various pressures. The values for the decoherence cross section obtained [see formula (6)] from these two plots are in agreement to within experimental error. From this we can conclude that inhomogeneous broadening plays a minor role, with an upper limit of 3×10^9 s^{-1}. This observation indicates that under these conditions, $T_2^{*2}\gg T_2'\tau$, confirming that the gas phase limit applies for delay times τ less than 1 ns for the I_2'–propane case presented.

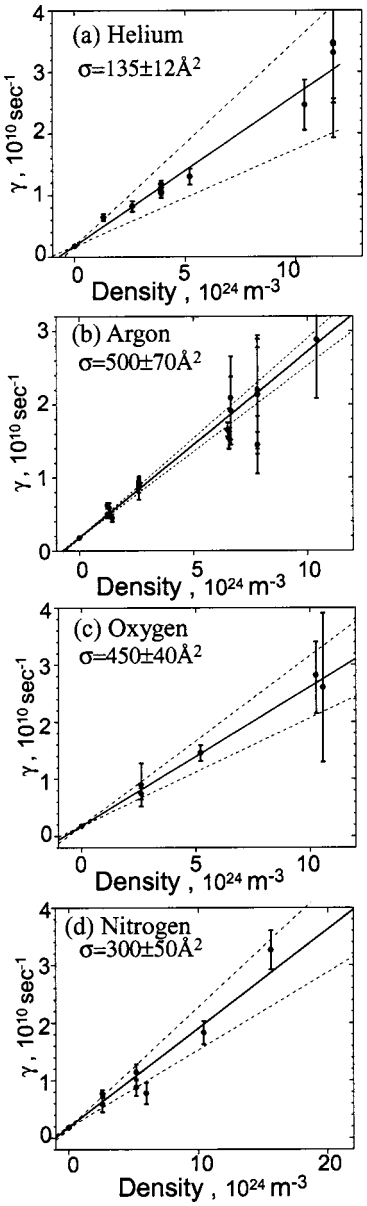

FIG. 5. Plots of homogeneous relaxation rate γ, of the PE signal with 50 fs excitation pulses, vs number density for (a) helium, (b) argon, (c) oxygen, and (d) nitrogen. Error bars indicate uncertainty in the fit. Error in the number density is smaller than the data points. The point at zero number density in each plot represents the relaxation rate of iodine at 5×10^{23} m^{-3} number density, and the uncertainty in this number is smaller than the data point in both dimensions.

V. DISCUSSION

The measurements of electronic coherence relaxation allow us to calculate cross sections. Assuming collisions occur at an average distance, R, determined by $\sigma=\pi R^2$, we can then calculate the average radius of interaction. The decoherence cross section for iodine–iodine collisions was measured

TABLE I. Parameters calculated for the long range interactions responsible for electronic coherence dephasing of I_2 molecules and buffer gases (M).

M	σ, Å^2	$R=\sigma^{1/2}/\pi^{1/2}$	v, ms^{-1} [e]	τ_i, ps	α,Å^3	IE, eV	C_6, J m^6 [g]	$C_{6\text{cal}}$, J m^6 [h]
He	135±12	6.5±1.5	1435	0.6	0.21[a]	24.619[a]	4.9×10^{-77}	0.306×10^{-77}
Ar	500±70	12±3.5	485	3.4	1.63[a]	15.781[a]	43.6×10^{-77}	2.061×10^{-77}
N_2	300±50	10±1.6	567	2.3	1.76[b]	15.581[c]	14.2×10^{-77}	2.215×10^{-77}
O_2	450±40	12±1.1	534	3.0	1.60[b]	12.0697[c]	36.9×10^{-77}	1.816×10^{-77}
C_3H_8	500±55	12±1.3	465	3.6	6.31[a]	10.962[a]	41.8×10^{-77}	6.861×10^{-77}
I_2[f]	1170±110	19±1.4	274	10.1	9[d]	9.307[c]	190×10^{-77}	9.046×10^{-77}

[a]D. A. McQuarrie and J. D. Simon, *Physical Chemistry* (University Science Books, Sausalito, California, 1997), p. 668.
[b]D. A. McQuarrie, *Statistical Mechanics* (University Science Books, Sausalito, California, 1997), p. 481.
[c]W. G. Mallard, *NIST Chemistry Webbook*, http://webbook.nist.gov/chemistry/ (2001).
[d]B. Friedrich, Phys. Rev. A, **61**, 025403 (2000).
[e]At 383 K.
[f]σ=1150±150 Å (Ref. 16); 590±110 Å (Ref. 26).
[g]Calculation with r^{-6} potential and experimental data.
[h]Calculation with formula for the dispersive force for parameters for iodine in the *X* state.

to be 1170 Å^2, giving us an interaction radius of $R=19$ Å. Notice that this value for the interaction radius is more than 10 Å greater than the van der Waals radius (see Fig. 8). Since we are dealing with the relaxation of electronic coherence, no energy needs to be exchanged by this interaction. Here we use a hard sphere model to describe these interactions, drawing an ''interaction region'' around the molecules in the coherence. We define this interaction region such that any molecule passing through it will produce at least a π shift in the phase of the electronic wave function of the iodine molecule.

The colliding partner, moving with a velocity in center-of-mass coordinates $\bar{v}$, interacts with an impact parameter *b*, the shortest distance between the two molecules during the interaction. The interaction potential $\Delta U(r)$ is a function of the distance between the two molecules, *r*, and it reflects the perturbation in the energy difference between the *B* and *X* electronic states of iodine caused by the buffer molecule (see Fig. 1).

If we picture the interaction region as a sphere around the iodine molecule, using the experimentally determined *R* (see Table I), we can estimate how long these dephasing interactions take, based on the average speed of the molecules, $\bar{v}$. The average time of each interaction assuming an average interaction length, $\bar{l}=(4/3)R$, is then given by $\bar{\tau}=\bar{l}/\bar{v}$. The values obtained using our measurements are compiled in Table I and range from 0.6 to 10 ps for helium and iodine, respectively. The intermolecular distances *R*, determined in this report, are graphically depicted in Fig. 8, while the molecules are represented as 98% electron density plots calculated using the Spartan molecular modeling program.[29] The above analysis of the experimental data shows that the interactions are long range when compared to the van der Waals radii, and short lived when compared to the lifetime of the electronic coherence.

As a plausible approximation, we assume the interactions to be dispersive and to follow an r^{-6} dependence, as obtained from the second term in the Lennard-Jones potential.[30] Based on the distance and weakness of the interaction we assume the molecules follow a linear path through the interaction region. The change in phase of the iodine wave function is then[31]

$$|\Delta\varphi(b)|=(2/\hbar)\int_0^\infty \Delta U(t)dt=3\pi C_6/(8\hbar\bar{v}b^5). \tag{7}$$

We can then calculate C_6 parameters for the I_2+M interactions, given in Table I using the formula,

$$C_6=(8/3)\bar{v}\hbar(\sigma/\pi)^{2.5}. \tag{8}$$

The values obtained are summarized in Table I and range from 4.9×10^{-77} to 190×10^{-77} J m^6 for helium and iodine, respectively.

In order to learn about the nature of the long-range dephasing collisions, we assume, that the intermolecular in-

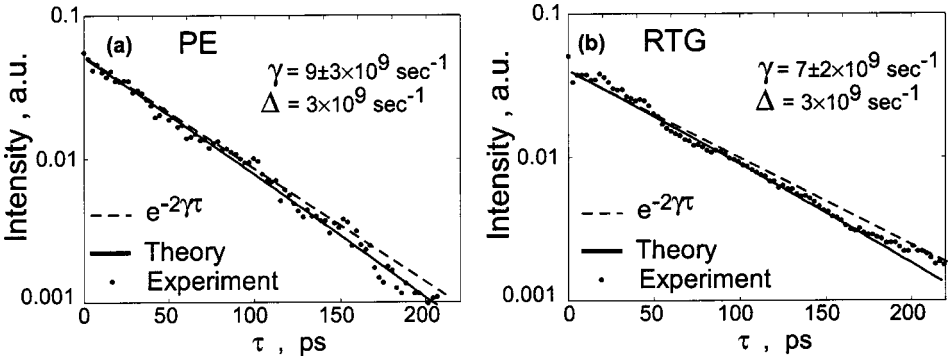

FIG. 6. Logarithmic plot of (a) PE and (b) RTG signals with 1200 fs excitation pulses, as a function of time (5×10^{23} m^{-3} iodine and 2.5×10^{24} m^{-3} propane at 400 K). Experimental data (dots) are fit (solid line) using the theory without approximations, Eqs. (1) and (2), presented in the text. The dashed line is a simulation based on a simple exponential decay with a homogeneous decay rate determined by the full fit.

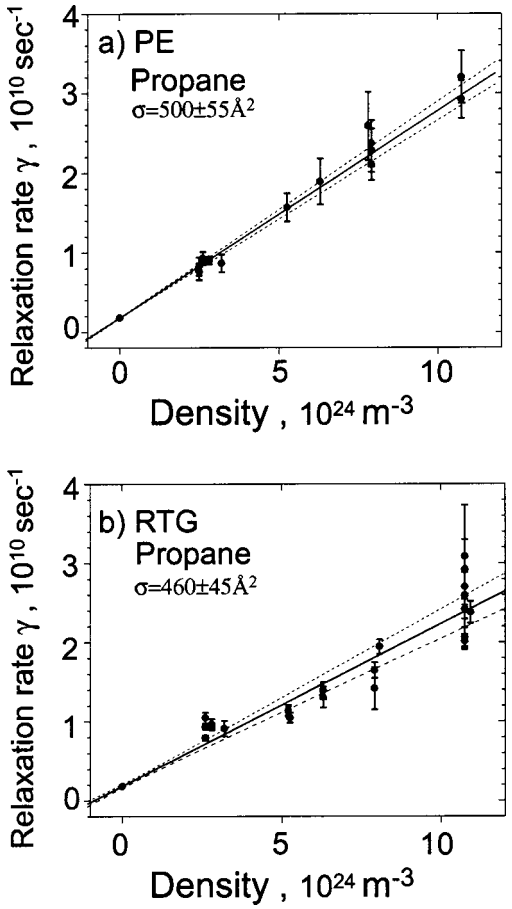

FIG. 7. Plot of the coherence relaxation rate γ vs pressure for propane buffer gas. Both photon echo data (a) and reverse transient grating data (b) are shown. The plots contain a total of 37 independent measurements. Error bars indicate uncertainty in the fit. Error in the number density is smaller than the data points. The point at zero number density in each plot represents the relaxation rate of iodine at $5\times10^{23}\,\mathrm{m}^{-3}$ number density, and the uncertainty in this number is smaller than the data point in both dimensions.

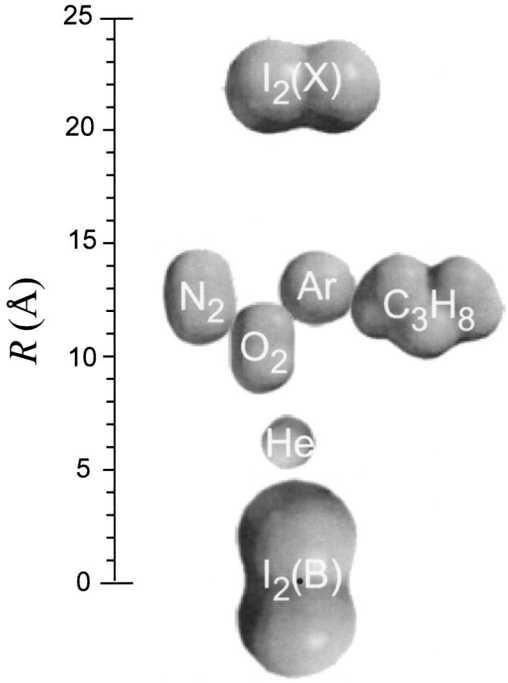

FIG. 8. Depiction of the distances R involved in the long-range interactions responsible for electronic coherence dephasing. Molecules are depicted as 98% electron density maps calculated using the Spartan molecular modeling program.

teraction is purely due to dispersion forces as a first-order approximation. We can calculate the dispersion parameter using and the expression,[30]

$$C_{6\mathrm{cal}}=(3/2)\alpha_1\alpha_2 I_1 I_2 (I_1+I_2)^{-1}, \tag{9}$$

where α_1 and α_2 are the ground state polarizabilities of the two molecules, and I_1 and I_2 are the ionization energies of the two molecules. The resulting values are summarized in Table I and are plotted in Fig. 9. Errors in the experimental numbers in Fig. 9 represent 2 standard deviations. Comparing the experimental to the calculated C_6 parameters in Fig. 9, we note that both follow a similar trend. There is about one order of magnitude difference between the two sets of parameters. This difference is primarily caused by the greater polarizability of the B state, a parameter that is not presently known, but is expected to be greater due to the B state's triplet character.

If we multiply the calculated points by 15, using the values obtained from the noble gases as guidelines (see open dots), we find that the simulation reproduces closely the observed trend and close agreement is observed for He, O_2, Ar, and I_2. Only the Lennard-Jones parameters for nitrogen and propane are a factor of 3 smaller. These smaller differences may be related to the absence of nonbonding electrons in these molecules. The factor of 15 increase in the polarizability of the excited state can be justified based on calculations of the polarizability of the ground and excited states of a number of small molecules.[32]

For our analysis we have considered and ruled out a number of processes that take place during collisions. Collision induced predissociation in iodine was studied

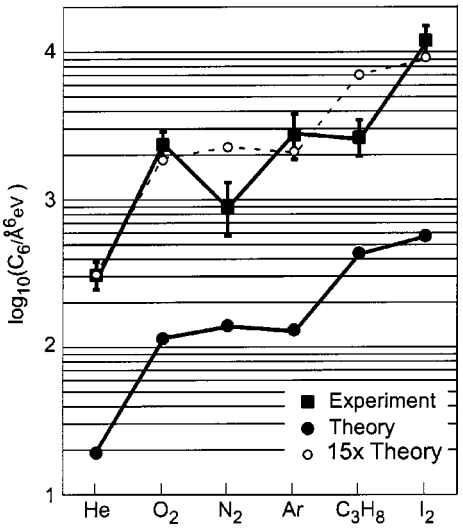

FIG. 9. Experimental (square points with uncertainties) and calculated (round black points) Lennard-Jones C_6 parameters for the buffer molecules in this study. Both data sets follow very similar trends, however experiment and theory values differ by a factor of 15. The round open points correspond to the calculated parameters multiplied by a factor of 15 to compensate for the greater excited state polarizability (see text).

previously.[33] The cross section for iodine–argon collision induced predissociation of the *B* state was measured to be 11.1 Å^2. This is 1/100 of the cross section of pure electronic dephasing, measured here, and for pressures less 1 atm can be assumed to be negligible. Collision-induced electronic state mixing for iodine–argon collision has also been studied.[34] The cross section for this process is of the same order of magnitude as the hard sphere (van der Waals) radius which is two orders of magnitude smaller than the dephasing cross section measured in our paper. Therefore this process is assumed to be negligible. Rotational-vibrational dephasing of iodine was also studied by, for example, Refs. 35, 36. It was shown that all these relaxations (actually intramolecular dephasing of rotational-vibrational wave packets) take place during the first several picoseconds (less than 15 ps for our spectral range of excitation) after excitation of the *B* state, an order of magnitude shorter time scale than our measurements (up to 200 ps). This type of intramolecular pulse relaxation was discussed in our previous work.[16]

The long-range interactions described in this report may involve other effects (quadrupole–induced dipole, quadrupole–quadrupole, etc.). Here we do not speculate beyond the fact that the experimentally derived values can be simulated by a model that only takes into account pure dispersion interaction estimates. Perhaps these measurements will encourage further theoretical analysis about the nature of these long range interactions.

VI. CONCLUSION

We have performed a number of photon echo measurements aimed at determining the electronic coherence dephasing time of gas phase iodine vapor, neat and in the presence of buffer gases. We have written the explicit dependence of the dephasing rate on the homogeneous and inhomogeneous contributions. With the full expression, we are able to calculate the dephasing time T_2' without assuming a gas or liquid phase limit. From the experimental decay rates, we have extracted dephasing cross sections and these are in good agreement with previous measurements in neat iodine.

We have verified the gas phase limit applies to the systems studied here, therefore only homogeneous relaxation plays a role and $\tau_{\mathrm{exp}}=1/(2\gamma)$. Our earlier work on iodine at lower densities had shown some intermediate behavior where inhomogeneous relaxation was overwhelming and the liquid phase limit applied.[16] It is interesting to note that the differences between quenching rates for the various buffer gases seem to have no dependence on the number of degrees of freedom available in the molecule, and only depends on the relative polarizabilities of the quenching species. The similarity between (for example, argon and propane) could be accounted for by the large distance of interaction and the modest amount of perturbation required to cause electronic dephasing.

In summary, we have determined the electronic coherence dephasing rates and cross sections for iodine molecules in buffer gases that range from low density to the condensed phase limit. We have limited our discussion about long-range interactions to simple descriptions. There are a number of theoretical issues that warrant further analysis.

ACKNOWLEDGMENTS

This research was funded by the Chemical Sciences, Geosciences, and Biosciences Division Office of Basic Energy Sciences, Office of Science, U.S. Department of Energy. M.D. is a Camille Dreyfus Teacher–Scholar.

[1] S. A. Rice, J. Chem. Phys. **409**, 422 (2001).
[2] N. E. Henriksen, Chem. Soc. Rev. **31**, 37 (2002).
[3] M. Dantus, Annu. Rev. Phys. Chem. **52**, 639 (2001).
[4] A. Assion, T. Baumert, M. Bergt, T. Brixner, B. Kiefer, V. Seyfried, M. Strehle, and G. Gerber, Science **282**, 919 (1998).
[5] P. Brumer and M. Shapiro, Acc. Chem. Res. **22**, 407 (1989).
[6] D. Deutsch and A. Ekert, Phys. World **11**, 47 (1998).
[7] C. H. Bennett and D. P. Divincenzo, Nature (London) **377**, 389 (1995).
[8] I. L. Chuang, R. Laflamme, P. W. Shor, and W. H. Zurek, Science **270**, 1633 (1995).
[9] R. Zadoyan, D. Kohen, D. A. Lidar, and V. A. Apkarian, Chem. Phys. **266**, 323 (2001).
[10] V. V. Lozovoy and M. Dantus, Chem. Phys. Lett. **351**, 213 (2002).
[11] E. V. Goldstein, O. Zobay, and P. Meystre, Phys. Rev. A **58**, 2373 (1998).
[12] M. Greiner, O. Mandel, T. Esslinger, T. W. Hansch, and I. Bloch, Nature (London) **415**, 39 (2002).
[13] V. V. Lozovoy, I. Pastirk, E. J. Brown, B. I. Grimberg, and M. Dantus, Int. J. Radiat. Phys. Chem. **19**, 531 (2000).
[14] V. V. Lozovoy, B. I. Grimberg, I. Pastirk, and M. Dantus, Chem. Phys. **267**, 99 (2001).
[15] V. V. Lozovoy, I. Pastirk, M. Comstock, and M. Dantus, Chem. Phys. **266**, 205 (2001).
[16] I. Pastirk, V. V. Lozovoy, and M. Dantus, Chem. Phys. Lett. **333**, 76 (2001).
[17] W. Zhang, V. Chernyak, and S. Mukamel, J. Chem. Phys. **110**, 5011 (1999).
[18] N. A. Kurnit, I. D. Abella, and S. R. Hartmann, Phys. Rev. Lett. **13**, 567 (1964).
[19] C. K. N. Patel and R. E. Slusher, Phys. Rev. Lett. **20**, 1087 (1968).
[20] I. Grimberg, V. V. Lozovoy, M. Dantus, and S. Mukamel, J. Phys. Chem. A **106**, 697 (2002).
[21] S. Mukamel, *Principles of Nonlinear Optical Spectroscopy* (Oxford University Press, New York, 1995).
[22] Y. Prior, Appl. Opt. **19**, 1741 (1980).
[23] J. A. Shirley, R. J. Hall, and A. C. Eckbreth, Opt. Lett. **5**, 380 (1980).
[24] J. Tellinghuisen, J. Chem. Phys. **58**, 2821 (1973).
[25] W. G. Mallard, *NIST Chemistry WebBook*, 2001.
[26] D. R. Lide, *Handbook of Chemistry and Physics*, 77th ed. (Chemical Rubber Company Press, Boca Raton, 1996–1997).
[27] E. T. Sleva and A. H. Zewail, Chem. Phys. Lett. **110**, 582 (1984).
[28] A. H. Zewail, T. E. Orlowski, K. E. Kones, and D. E. Godar, Chem. Phys. Lett. **48**, 256 (1977).
[29] Spartan Version 5.1.3; 6-31G* electron density calculation.
[30] J. D. Simon and D. A. MacQuarrie, *Physical Chemistry: A Molecular Approach* (University Science Books, Sausalito, 1997).
[31] R. Kubo, in *Fluctuation, Relaxation, and Resonance in Magnetic Systems* (Oliver and Boyd, London, 1961).
[32] P. Fuentealba, Y. Simon-Manso, and P. Chattaraj, J. Phys. Chem. A **104**, 3185 (2000).
[33] C. Lienau and A. H. Zewail, J. Phys. Chem. **100**, 18629 (1996).
[34] Q. Liu, C. Wan, and A. H. Zewail, J. Phys. Chem. **100**, 18666 (1996).
[35] M. Gruebele and A. H. Zewail, J. Chem. Phys. **98**, 883 (1993).
[36] A. H. Zewail, M. Dantus, M. Bowman, and M. Gruebele, J. Photochem. Photobiol., A **62**, 301 (1992).